

Ultrathin Carbon Nanosheets for Highly-efficient Capacitive K-ion and Zn-ion Storage

Yamin Zhang ^{b, c}, Zhongpu Wang ^b, Deping Li ^{a, b *}, Qing Sun ^b, Kangrong Lai ^c, Kaikai Li ^a,
Qunhui Yuan ^a, Xingjun Liu ^a and Lijie Ci ^{a, b *}

^a State Key Laboratory of Advanced Welding and Joining, School of Materials Science and Engineering, Harbin Institute of Technology, Shenzhen, 518055, China

^b Research Center for Carbon Nanomaterials, Key Laboratory for Liquid-Solid Structural Evolution & Processing of Materials (Ministry of Education), School of Materials Science and Engineering, Shandong University, Jinan, 250061, China

^c Department of Physics, Changji University, Changji 831100, China

Address correspondence to cilijie@hit.edu.cn; lidedping@hit.edu.cn

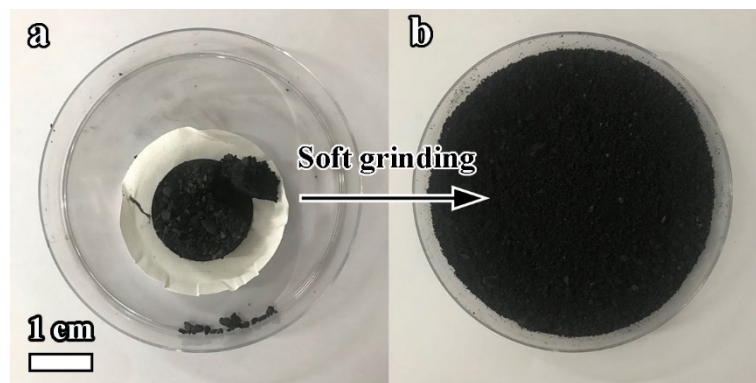


Figure S1 Optical images of samples (a) before and (b) after “soft-grinding” process.

The obtained carbonaceous samples stay in a soft-aggregation state after washing, filtration and drying processes. Therefore, we introduce a “soft-grinding” process to obtain well-dispersed powders for preparing uniform slurries of electrodes.

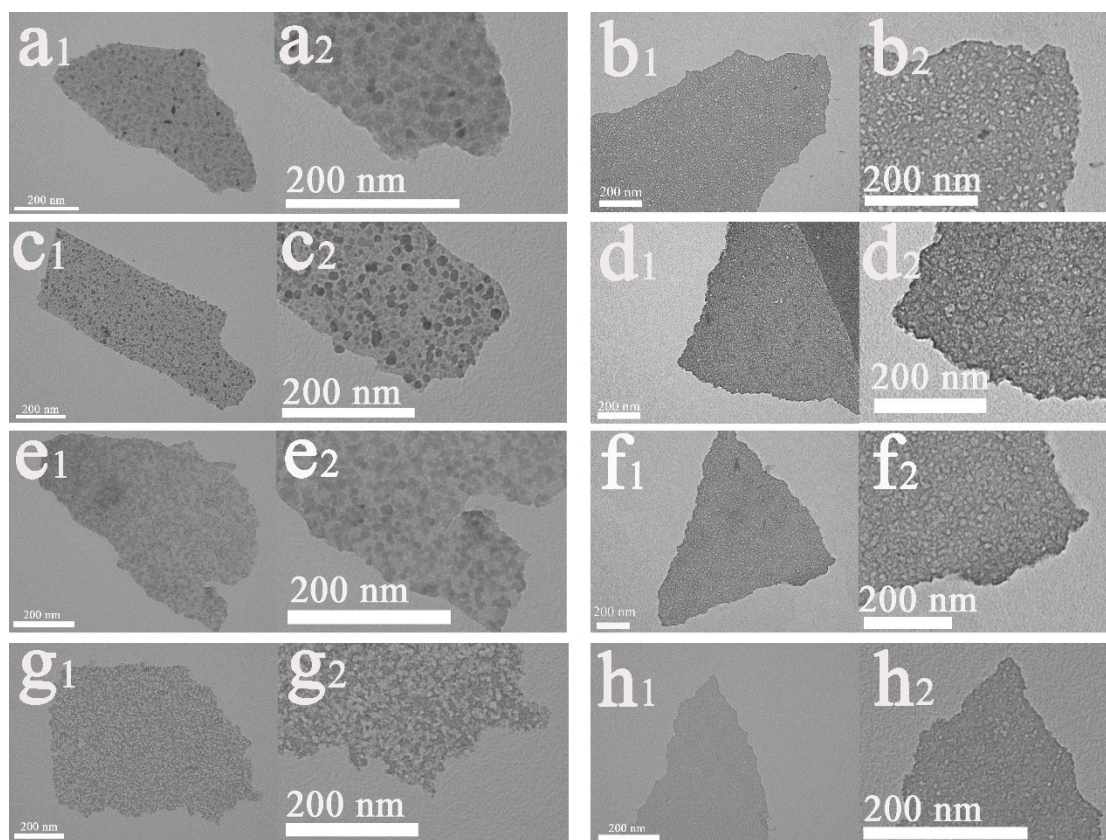


Fig. S2 TEM images of the calcined precursors (a) Ca-600-P; (c) Ca-700-P; (e) Ca-800-P; (g) Ca-1000-P and obtained carbons (b) Ca-600; (d) Ca-700; (f) Ca-800; (h) Ca-1000

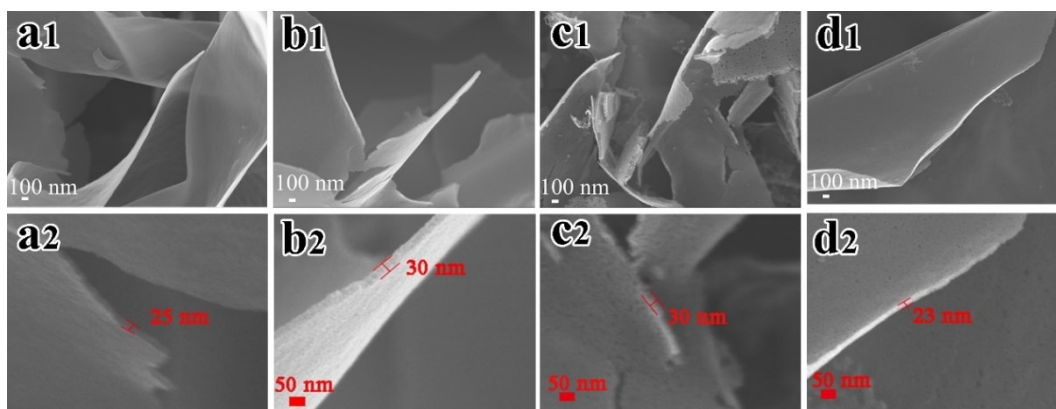


Fig. S3 SEM image of Ca-x, (a) Ca-600; (b) Ca-700; (c) Ca-800; (d) Ca-1000

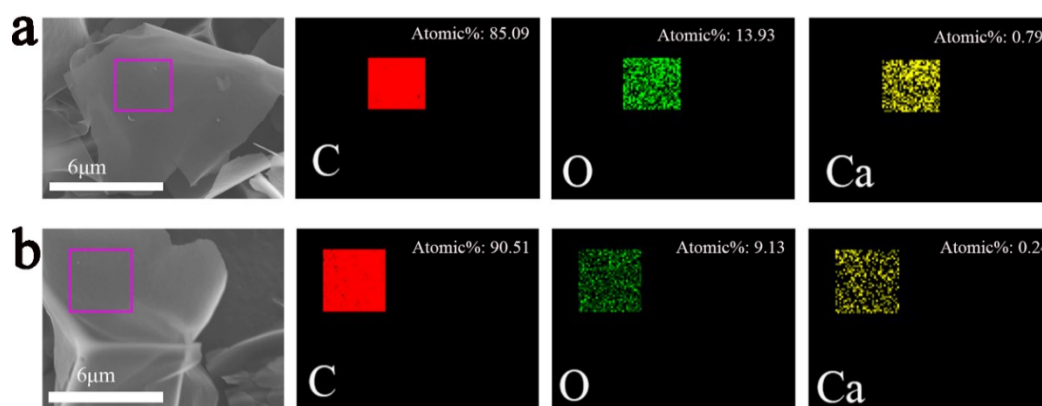


Fig. S4 SEM images and corresponding elemental mapping of C, O and Ca elements. (a) Ca-600 and (b) Ca-900

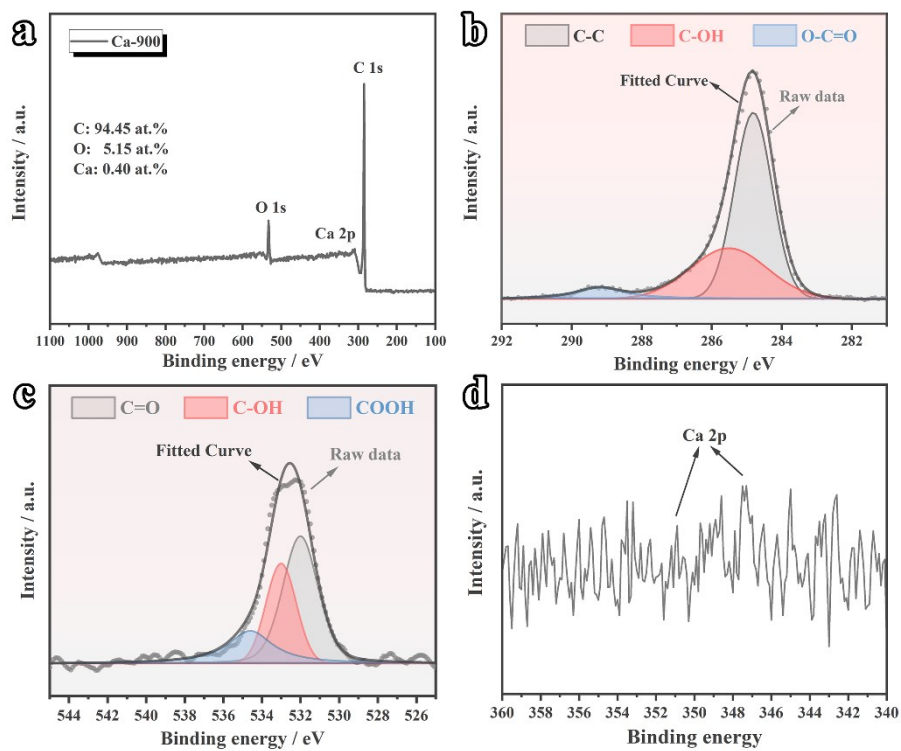


Fig. S5 XPS spectrum of Ca-900. (a) Survey spectrum, (b) C 1s, (c) O 1s, (d) Ca 2p.

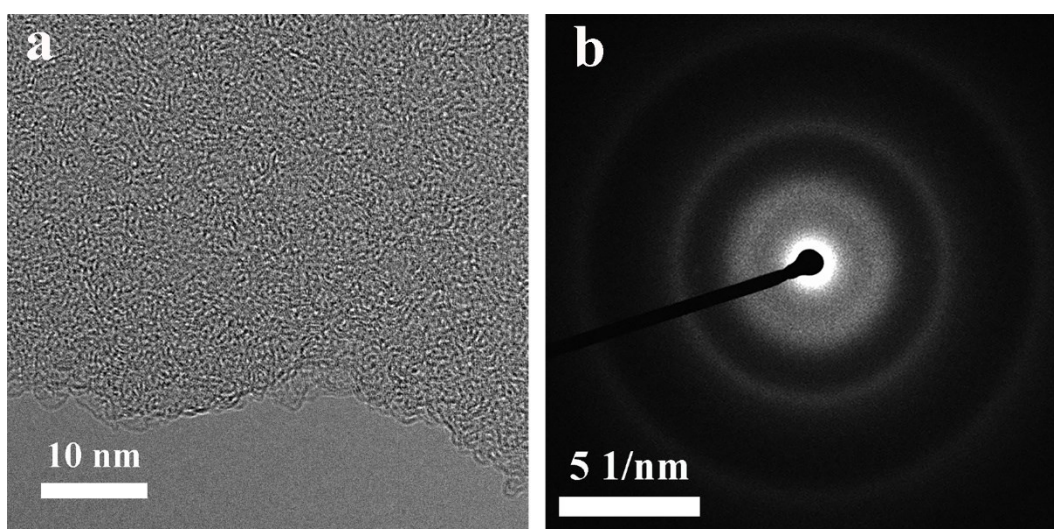


Fig. S6 (a) HRTEM image and (b) SAED pattern of Ca-900.

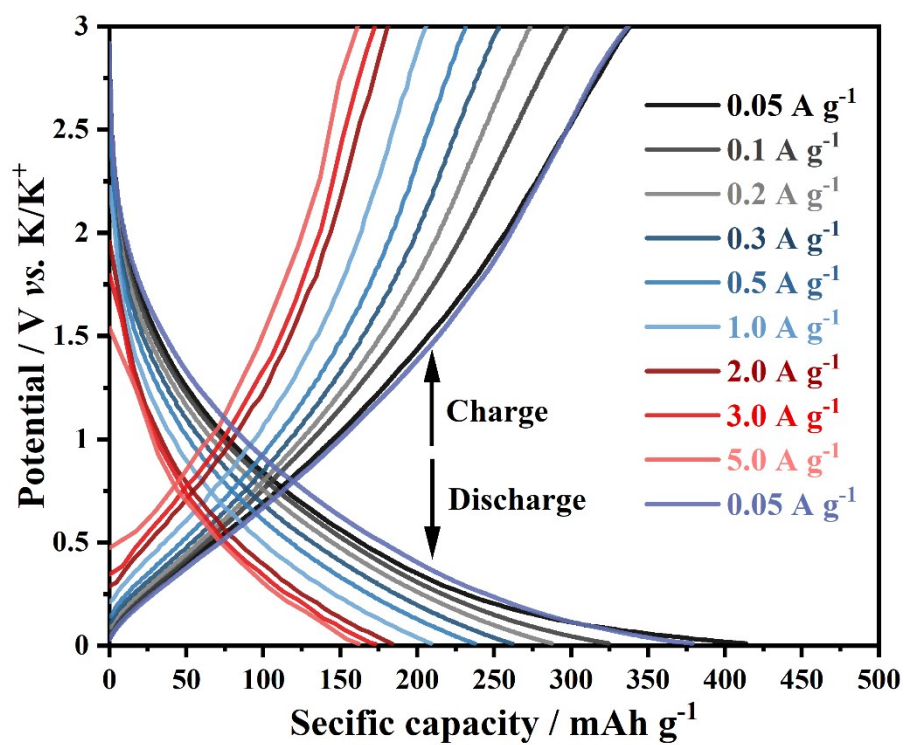


Fig. S7 GCD profiles of Ca-900.

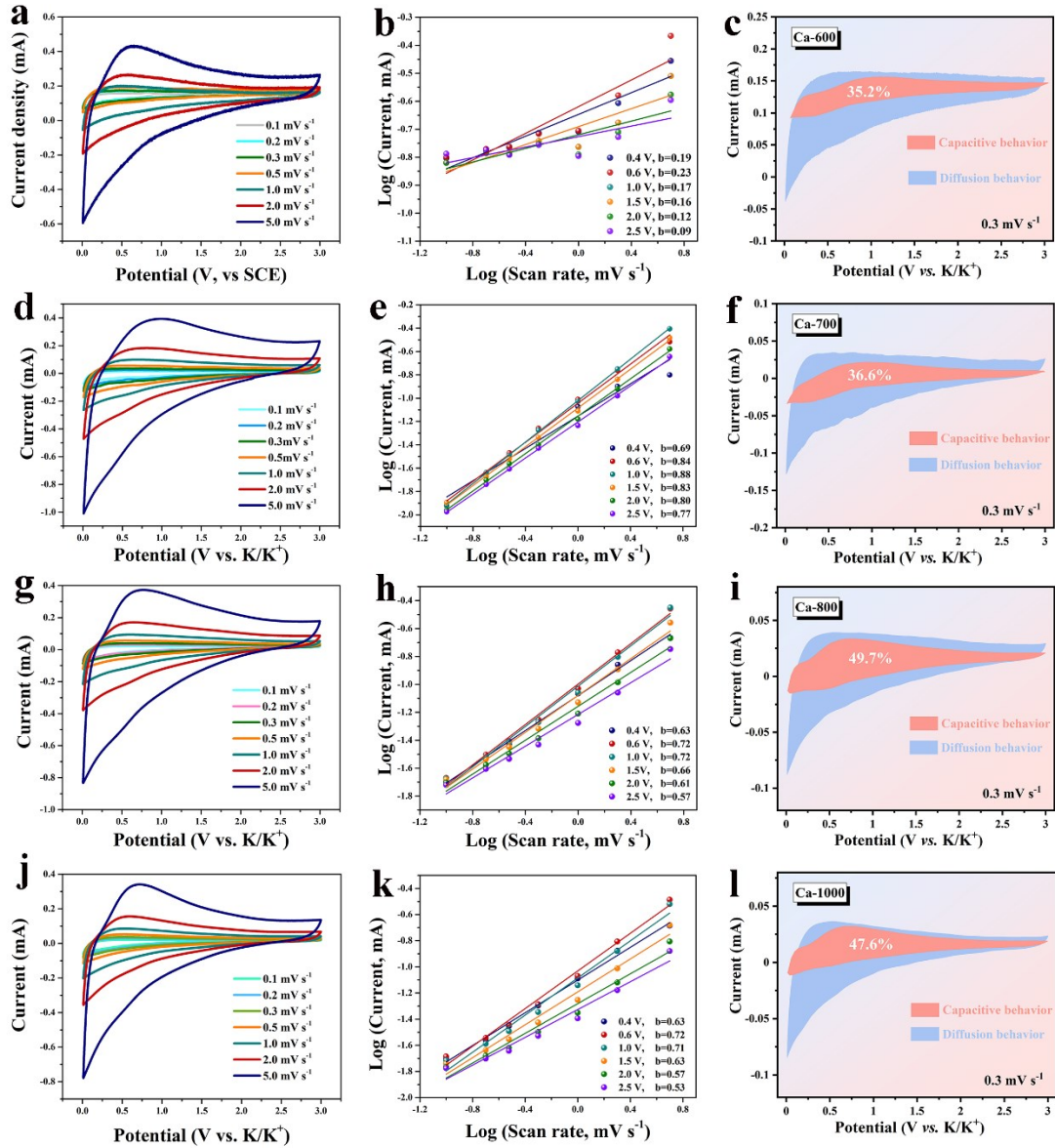


Fig.S8 Kinetic analysis of K-ion storage behavior of Ca-x electrodes. CV curves at various scan rates, (a) Ca-600, (c) Ca-700, (g) Ca-800, (j) Ca-1000. *b* values determined at various potassiation depths, (b) Ca-600, (e) Ca-700, (h) Ca-800, (k) Ca-1000. Sketch of the capacitive contribution ratio at 1.0 mV s^{-1} , (c) Ca-600, (f) Ca-700, (i) Ca-800, (l) Ca-1000

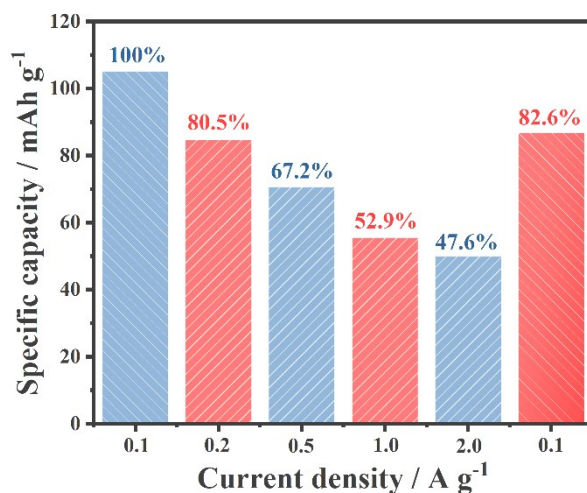


Fig. S9 Capacity retention ratios of Ca-900//Zn.

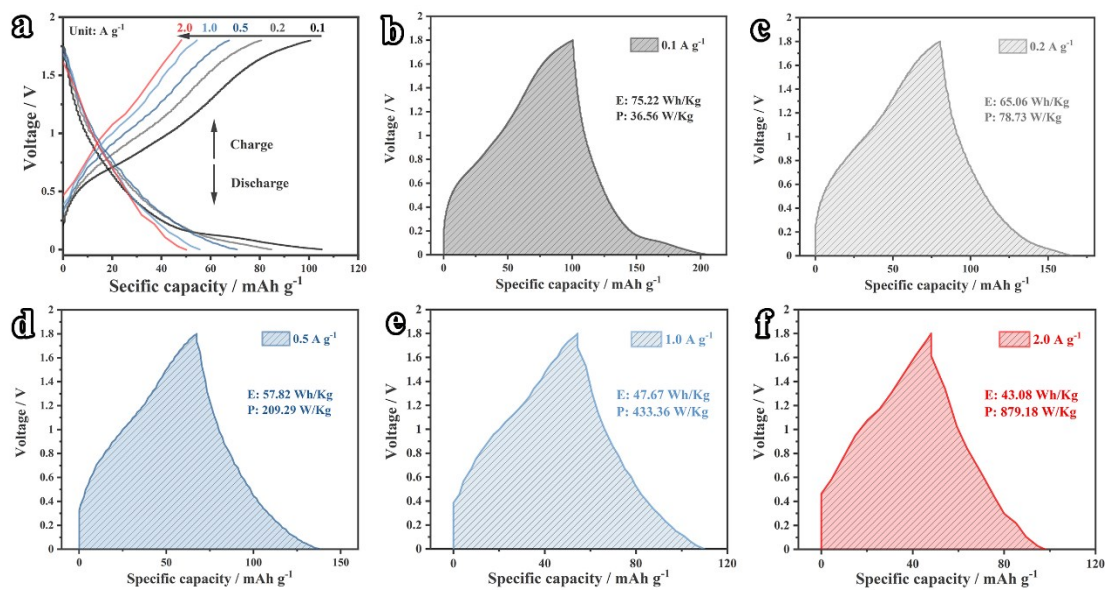


Fig. S10 (a) GCD profiles at current densities from 0.1 to 2.0 A g⁻¹. (b-f) Sketch diagram for energy density/power density calculations.

As depicted in Figure S10, we combined the charge and discharge curve together to obtain a quasi-triangle area, and the energy density is based on half the value of the area. For example, the area of the shadow area in Figure S10a is ~150.44, then the energy density can be extracted as ~75.22 Wh/Kg. Power density can be calculated by the formula: $P=E/t$, while the value of t can be obtained by the formula: $t=\text{capacity}/\text{current density}$.

Table. S1 Survey of SSA and pore volume.

| Sample | SSA (m ² g ⁻¹) | Total pore volume (cm ³ g ⁻¹) | Micro-pore volume (cm ³ g ⁻¹) | Meso-pore volume (cm ³ g ⁻¹) | Macro-pore volume (cm ³ g ⁻¹) |
|---------|--|---|--|---|--|
| Ca-600 | 192.02 | 0.18065/100% | 0.03893/21.5% | 0.12259/67.9% | 0.01913/10.6% |
| Ca-700 | 270.02 | 0.65515/100% | 0.46066/70.3% | 0.19053/29.1% | 0.00396/0.6% |
| Ca-800 | 835.46 | 0.56530/100% | 0.22297/39.4% | 0.33452/59.2% | 0.00781/1.4% |
| Ca-900 | 955.08 | 1.08586/100% | 0.20298/18.6% | 0.87144/80.3% | 0.01145/1.1% |
| Ca-1000 | 1414.93 | 0.94460/100% | 0.41306/43.7% | 0.51654/54.7% | 0.01500/1.6% |

A higher SSA always contributes to higher capacitive behavior, however, this is not a linear relationship, which means that not all surfaces can be totally utilized for metal-ion storage. For example, inherently tortuous micropores can provide high SSA and contributes to high capacitive behavior. However, sluggish ion transportation occurs simultaneously, which induces poor rate performance. Besides, the tortuous micropores may induces “pore-blocking effect”, which will trap the stored ions and lead to low reversibility (low coulombic efficiency). Therefore, it is very important to balance the ratios of micropores, mesopores and macropores.^{1,2} Specifically, sufficient mesopores and macropores can ensure the deep permeation of the electrolyte, which can help utilize the surface of micropores. Besides, a large proportion of mesopores can serve as fast ion transportation channels, alleviating the “pore-blocking effect” and provide surfaces for ion adsorption. Moreover, the ionic size of Zn-ion is 0.74 nm (0.86 nm for hydrated Zn-ion), while Ca-1000 shows abundant micropores at ~0.55 nm (Figure 4b), the dis-match of pore size and ion radius also emphasize the importance of balancing the size and ratio of pores.

Overall, Ca-900 with relatively high SSA and high ratio of mesopores exhibit the best electrochemical performance (as concluded in Table S1). Compared with Ca-900, although Ca-1000 has higher SSA, its higher ratio of micropores indicates a higher tortuous degree and suffers severe “pore-blocking effect”. Therefore, Ca-1000 cannot exert its full potential, which also illuminates the importance of balancing the ratios of various pores for carbon-based electrode materials.

Table. S2 A survey of the recently reported carbonaceous electrodes in PIBs

| Anode materials | Electrolyte | Reversible capacity & rate capability | Cycling stability | Ref |
|---|---------------------------------------|--|---|-----------|
| Ultrathin porous carbon nanosheets | 0.8 M KPF ₆ in EC:DEC(1:1) | 430.7 mAh g ⁻¹ @ 50 mA g ⁻¹ 154.8 mAh g ⁻¹ @ 5000 mA g ⁻¹ | 126.4 mAh g ⁻¹ (~81.2% after 4000 cycles @ 1000 mA g ⁻¹) | This work |
| Graphitic nanocarbons | 0.8 M KPF ₆ in EC:DEC(1:1) | 280 mAh g ⁻¹ @ 50 mA g ⁻¹ 56.6 mAh g ⁻¹ @ 5000 mA g ⁻¹ | 189 mAh g ⁻¹ (75.4% after 200 cycles @ 200 mA g ⁻¹) | 3 |
| Porous N-doped carbon fibers | 1 M KPF ₆ in EC:DMC (1:1) | 197 mAh g ⁻¹ @ 50 mA g ⁻¹ 57.0 mAh g ⁻¹ @ 250 mA g ⁻¹ | 65 mAh g ⁻¹ (65.9% after 346 cycles @ 100 mA g ⁻¹) | 4 |
| carbon nanospheres | 0.8 M KPF ₆ in EC:DEC(1:1) | 365.5 mAh g ⁻¹ @ 200 mA g ⁻¹ 137.0 mA h g ⁻¹ @ 4000 mA g ⁻¹ | 109.8 mAh g ⁻¹ (66.0% after 5000 cycles @ 2000 mA g ⁻¹) | 5 |
| Nitrogen-doped carbon nanosheets | 0.8 M KPF ₆ in EC:DEC(1:1) | 367 mAh g ⁻¹ @ 50 mA g ⁻¹ 168 mAh g ⁻¹ @ 2000 mA g ⁻¹ | 225 mAh g ⁻¹ (70.5% after 1000 cycles @ 500 mA g ⁻¹) | 6 |
| S/O co-doped Porous Hard Carbon Microspheres | 0.8 M KPF ₆ in EC:DEC(1:1) | 230 mAh g ⁻¹ @ 50 mA g ⁻¹ 158 mA h g ⁻¹ @ 1000 mA g ⁻¹ | 108.4 mA h g ⁻¹ (72.2% after 2000 cycles @ 1000 mA g ⁻¹) | 7 |
| Graphitic carbon | 0.8 M KPF ₆ in EC:DEC(1:1) | 221 mAh g ⁻¹ @ 20 mA g ⁻¹ 13.6 mAh g ⁻¹ @ 1000 mA g ⁻¹ | 72 mA h g ⁻¹ (50% after 240 cycles @ 100 mA g ⁻¹) | 8 |
| Nitrogen doped carbon nanofibers | 0.8 M KPF ₆ in EC:DEC(1:1) | 248 mAh g ⁻¹ @ 25 mA g ⁻¹ 101 mAh g ⁻¹ @ 20000 mA g ⁻¹ | 146 mAh g ⁻¹ (73.0% after 4000 cycles @ 2000 mA g ⁻¹) | 9 |
| Graphitic carbons | 1 M KPF ₆ in EC:DMC (1:1) | 100 mAh g ⁻¹ @ 100 mA g ⁻¹ 89 mAh g ⁻¹ @ 10000 mA g ⁻¹ | 246 mAh g ⁻¹ (95% after 1000 cycles @ 100 mA g ⁻¹) | 10 |
| P/O dual-doped graphene | 1 M KPF ₆ in EC:DMC (1:1) | 385 mAh g ⁻¹ @ 500 mA g ⁻¹ 160 mAh g ⁻¹ @ 2000 mA g ⁻¹ | 160 mAh g ⁻¹ (80% after 600 cycles @ 2000 mA g ⁻¹) | 11 |
| Hierarchical porous yolk-shell carbon sphere | 0.8 M KPF ₆ in EC:DEC(1:1) | 314 mAh g ⁻¹ @ 50 mA g ⁻¹ 155 mAh g ⁻¹ @ 1000 mA g ⁻¹ | 138 mAh g ⁻¹ (93% after 1200 cycles @ 100 mA g ⁻¹) | 12 |
| Wing-like porous carbon sheets | 1 M KPF ₆ in EC:DEC(1:1) | 347 mAh g ⁻¹ at 50 mA g ⁻¹ 122 mAh g ⁻¹ at 20 A g ⁻¹ | 118 mAh g ⁻¹ (87% after 4000 cycles @ 2000 mA g ⁻¹) | 13 |

References

1. Merlet, C.; Rotenberg, B.; Madden, P. A.; Taberna, P.-L.; Simon, P.; Gogotsi, Y.; Salanne, M., On the molecular origin of supercapacitance in nanoporous carbon electrodes. *Nature Materials* **2012**, *11* (4), 306-310.
2. Zhang, L.; Yang, X.; Zhang, F.; Long, G.; Zhang, T.; Leng, K.; Zhang, Y.; Huang, Y.; Ma, Y.; Zhang, M.; Chen, Y., Controlling the Effective Surface Area and Pore Size Distribution of sp² Carbon Materials and Their Impact on the Capacitance Performance of These Materials. *Journal of the American Chemical Society* **2013**, *135* (15), 5921-5929.
3. Zhang, W.; Ming, J.; Zhao, W.; Dong, X.; Hedhili, M. N.; Costa, P. M.; Alshareef, H. N., Graphitic Nanocarbon with Engineered Defects for High-Performance Potassium-Ion Battery Anodes. *Advanced Functional Materials* **2019**, *29* (35), 1903641.
4. Zhang, M.; Shoaib, M.; Fei, H.; Wang, T.; Zhong, J.; Fan, L.; Wang, L.; Luo, H.; Tan, S.; Wang, Y., Hierarchically Porous N-Doped Carbon Fibers as a Free-Standing Anode for High-Capacity Potassium-Based Dual-Ion Battery. *Advanced Energy Materials* **2019**, *9* (37), 1901663.
5. Wang, G.; Xiong, X.; Xie, D.; Lin, Z.; Zheng, J.; Zheng, F.; Li, Y.; Liu, Y.; Yang, C.; Liu, M., Chemically activated hollow carbon nanospheres as a high-performance anode material for potassium ion batteries. *Journal of Materials Chemistry A* **2018**, *6* (47), 24317-24323.
6. Liu, L.; Chen, Y.; Xie, Y.; Tao, P.; Li, Q.; Yan, C., Understanding of the Ultrastable K-Ion Storage of Carbonaceous Anode. *Advanced Functional Materials* **2018**, *28* (29), 1801989.
7. Chen, M.; Wang, W.; Liang, X.; Gong, S.; Liu, J.; Wang, Q.; Guo, S.; Yang, H., Sulfur/Oxygen Codoped Porous Hard Carbon Microspheres for High-Performance Potassium-Ion Batteries. *Advanced Energy Materials* **2018**, *8* (19), 1800171.
8. Xing, Z.; Qi, Y.; Jian, Z.; Ji, X., Polyanocrystalline graphite: a new carbon anode with superior cycling performance for K-ion batteries. *ACS applied materials & interfaces* **2016**, *9* (5), 4343-4351.
9. Xu, Y.; Zhang, C.; Zhou, M.; Fu, Q.; Zhao, C.; Wu, M.; Lei, Y., Highly nitrogen doped carbon nanofibers with superior rate capability and cyclability for potassium ion batteries. *Nature communications* **2018**, *9* (1), 1720.
10. Cohn, A. P.; Muralidharan, N.; Carter, R.; Share, K.; Oakes, L.; Pint, C. L., Durable potassium ion battery electrodes from high-rate cointercalation into graphitic carbons. *Journal of Materials Chemistry A* **2016**, *4* (39), 14954-14959.
11. Ma, G.; Huang, K.; Ma, J.-S.; Ju, Z.; Xing, Z.; Zhuang, Q.-c., Phosphorus and oxygen dual-doped graphene as superior anode material for room-temperature potassium-ion batteries. *Journal of Materials Chemistry A* **2017**, *5* (17), 7854-7861.
12. Zhang, H.; He, H.; Luan, J.; Huang, X.; Tang, Y.; Wang, H., Adjusting the yolk-shell structure of carbon spheres to boost the capacitive K⁺ storage ability. *Journal of Materials Chemistry A* **2018**, *6* (46), 23318-23325.
13. Cui, Y.; Liu, W.; Wang, X.; Li, J.; Zhang, Y.; Du, Y.; Liu, S.; Wang, H.; Feng, W.; Chen, M., Bioinspired Mineralization under Freezing Conditions: An Approach to Fabricate Porous Carbons with Complicated Architecture and Superior K⁺ Storage Performance. *ACS Nano* **2019**, *2019*.